Mediterranean Journal of Basic and Applied Sciences (MJBAS)
Volume 7, Issue 2, Pages 103-115, April-June 2023

Spectral Attributes in Onshore Fuba Field Niger-Delta, Nigeria, Using 3-D Seismic Time-lapse Data

U. Ochoma*

Department of Physics, Rivers State University, P.M.B 5080, Port Harcourt, Nigeria.
*Email: umaocho@gmail.com**

DOI: https://doi.org/10.46382/MJBAS.2023.7213

Article Received: 09 April 2023 *Article Accepted: 28 May 2023* *Article Published: 13 June 2023*

ABSTRACT

Spectral attributes in Onshore Fuba Field Niger Delta, Nigeria, are here presented, using 3D seismic time-lapse data. The FUBA Field lies on latitudes $4^0$50'58''- $4^0$55'19''N and longitudes $6^0$18'41''- $6^0$26'41''E with aerial extent of 840km^2**.** The base (1997) and the monitor (2009) seismic surveys resulted in a 4D response difference. The Base and Monitor data have a root-mean-square repeatability ratio (RRR) of 0.38 implying a very good repeatability when considering the acquisition, processing and environmental noises. Data processing and interpretation were carried out using Petrel software. Reservoir pressure decline rate of 0.062psi/day resulted in production decline rate of 1192.21bbl/day. Structural interpretation of seismic data reveals a highly faulted field. Two distinct horizons were mapped. Fault and horizon interpretation shows closures that are collapsed crestal structures bounded by two major faults. All the interpreted faults are normal synthetic and antithetic faults which are common in the Niger Delta basin. The depth structure maps reveal anticlinal faults. Reservoirs are found at a shallower depth from 6500 to 7500 ft and at a deeper depth ranging from 11500 to 13000 ft. The variance values range from 0.0 to 1.0. The Variance edge analysis was used to delineate the prominent and subtle faults in the area. The results of spectral decomposition at the different frequencies indicates areas of low frequency and high amplitude associated with known hydrocarbon zones, meandering channels, lobes and the presence of small scale faults in the field. The results of the work will help in the recovery of more hydrocarbon as by-passed zones and subtle structures are revealed in the area of study.

Keywords: Seismic, Time-lapse, Faults, Spectral decomposition, Meandering channels, Niger Delta, Nigeria.

1.0. Introduction

Spectral decomposition is the use of small or short windows for transforming and displaying frequency/ wavenumber spectra (Sheriff, 2002). Spectral analysis has been one of the significant interpretation methods in seismic analysis because seismic data is non-stationary in nature (Bayowa, et al, 2021). Compared with horizon based slices in time domain, it provides better vertical resolution of various depositional features on frequency slices (Naseer, and Asim, 2018; Tayyab, et al, 2017). Spectral decomposition can be done by using different methods such as short window discreet Fourier transform, Continuous wavelet transform, stock-well transform, matching pursuit or by using Fast Fourier Transform (Cohen, 1995; Castagna, and Sun, 2006). The information could be used to detect, characterize, predict and keep under surveillance the hydrocarbon reservoirs (Taner et al, 1979). Several researchers have made enormous contributions based on spectral analysis within the Niger Delta basin to investigate the potentiality of hydrocarbon deposits. Marfurt, and Kirlin, (2001) used the Discrete Fourier Transform to map time thicknesses. Castagna, et al, (2003) and Sinha et al, (2005) applied spectral decomposition as a direct hydrocarbon indicator. Tomasso, et al, (2010) used spectral re-composition to recover the frequencies and its associated amplitudes (weights) as a reversed problem by an improved formula.

This study is taken from Fuba Field, Depobelt, Niger Delta, Nigeria. The ultimate deliverable of this study was spectral attributes, using 3-D seismic time-lapse data. The major components of this study are: (a) Well Correlation performed in order to determine the continuity of the reservoir sand across the field. (b) Seismic Interpretation which involves differencing of seismic volume, well-to-seismic tie, fault mapping, horizon mapping, time surface generation, depth conversion and seismic attributes generation. This aids in giving more insight into spectral attributes in onshore Fuba field Niger-Delta, Nigeria, using 3-D seismic time-lapse data.

Mediterranean Journal of Basic and Applied Sciences (MJBAS)
Volume 7, Issue 2, Pages 103-115, April-June 2023

2.0. Location and Geology of the Study Area

The proposed study area Fuba Field is located in the onshore Niger Delta region. Figure 1 shows the map of the Niger Delta region showing the study area. The Niger Delta lies between latitudes 4° N and 6° N and longitudes 3° E and 9° E (Whiteman, 1982). The Delta ranks as one of the major oil and gas provinces globally, with an estimated ultimate recovery of 40 billion barrels of oil and 40 trillion cubic feet of gas (Adegoke, et al., 2017). The coastal sedimentary basin of Nigeria has been the scene of three depositional cycles (Short, and Stauble, 1967).

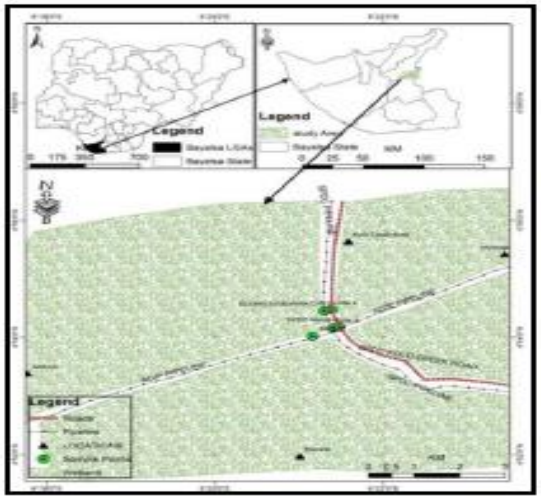

Figure 1. Map of Niger Delta Oilfields showing the location of Fuba Field

The first began with a marine incursion in the middle Cretaceous and was terminated by a mild folding phase in Santonian time. The second included the growth of a proto-Niger delta during the Late Cretaceous and ended in a major Paleocene marine transgression. The third cycle, from Eocene to Recent, marked the continuous growth of the main Niger delta. A new threefold lithostratigraphic subdivision is introduced for the Niger delta subsurface, comprising an upper sandy Benin Formation, an intervening unit of alternating sandstone and shale named the Agbada Formation, and a lower shaly Akata Formation. These three units extend across the whole delta and each ranges in age from early Tertiary to Recent. They are related to the present outcrops and environments of deposition. A separate member of the Benin Formation is recognized in the Port Harcourt area. It is Miocene-Recent in age with a minimum thickness of more than 6,000ft (1829m) and made up of continental sands and sandstones (>90%) with few shale intercalations (Horsfall, et al., 2017). Subsurface structures are described as resulting from movement under the influence of gravity and their distribution is related to growth stages of the delta (Ochoma, et al., 2020). Rollover anticlines in front of growth faults form the main objectives of oil exploration, the hydrocarbons being found in sandstone reservoirs of the Agbada Formation.

3.0. Methodology

3.1. Normalized Root Mean Square (NRMS) Repeatability (RRR) and Differencing of Seismic Volume

Pre-stack time migrated full-offset 3D and 4D stacks were available. The success of time-lapse reservoir monitoring depends on removing the non-repeatable effects such as configurations, seasonal changes, atmospheric temperatures, tides, elastic properties of the overburden, compaction, multiples, and rock heterogeneities (Vedanti,

et al., 2009; Varela, et al., 2006). Obstructions, weather patterns, cost constraints, and maritime traffic can also influence the survey orientation. Having considered the above sources of error in repeatability, the acquisition system itself, positioning accuracy, receiver sensitivity/calibration, and source calibration must also be looked into. All these sources of error were handled through normalized root mean square (NRMS) analysis. The NRMS value is simply the RMS amplitude of the difference, normalized by the average of the RMS amplitudes of the baseline data Baseline and monitor data Monitor (Kragh, and Christie, 2002):

$$NRMS = -\frac{2\,rms(Monitor - baseline)}{rms(Monitor) + (Baseline)} \quad (1)$$

$$rms = \sqrt{\frac{\sum x_i^2}{N}} \quad (2)$$

The summation is over N number of all samples x_i (i = 1, 2, · · ·, N) in the time window.

The NRMS value is a measure of non-repeatability. If NRMS = 0, the data are perfectly repeatable. Typical "good" values of NRMS quoted in the literature range from 0.1 to 0.3 [10% to 30% non-repeatability] (Johnston, 2013).

Monitor 4D seismic volume was subtracted from the Base 3D volume, and the differences was interpreted to determine the areas of the field that have been changed during production. Areas of the areas in the field where there have been changes were analyzed and compared to production activity in those areas.

3.2. Well-to-Seismic Ties

Well correlation is the first stage of the pre-interpretation process. The process of well correlation involves lithologic description, picking top and base of sand-bodies, fluid discrimination and then linking these properties from one well to another based on similarity in trends. In between these two lithologies in the subsurface, the gamma ray log is often used. Correlation of reservoir sands was achieved using the top and base of reservoir sands picked. The correlation process was possible based on similarity in the behavior of the gamma ray log the Niger Delta; the predominant lithologies are sands and shales. In order to discriminate shapes. Also, the thickness of the shale bodies overlying and underlying the sand body is considered during Correlation. After defining the lithologies, the resistivity log was used for discriminating the type of fluid occurring within the pores in the rocks.

There are eight basic steps involved in seismic interpretation relevant to this study and they include; Differencing of seismic volume, Well-to-seismic ties, Fault Mapping, Horizon mapping, Time surface generation, velocity Modelling, Depth Conversion and attributes generation. Well-to-seismic tie is a process that enables the visualization of well information on seismic data. For this process to be achieved, the following are basic requirements; checkshot, sonic log, density log and a wavelet. The sonic log, which is the reciprocal of velocity, was calibrated using the checkshot data. The calibration process is necessary in order to improve the quality of the sonic log because the sonic log is prone to washouts and other wellbore related issues. The results of calibrating the sonic log with the checkshot gives a new log called the calibrated sonic log.

The calibrated sonic log is used along with the density log to generate an acoustic impedance (AI) log. The acoustic impedance log is calculated for each layer of rock. The next step involves generating the reflectivity

coefficient (RC) log. The RC is calculated and generated using the AI log. The RC log generated is then convolved with a wavelet to generate a synthetic seismogram which is comparable with the seismic data. The statistical wavelet utilized for convolution is extracted from the seismic data. The synthetic seismogram was generated for every well that had checkshot, density and sonic log. The reflections on the synthetic seismogram were matched with the reflections on seismic data. The mathematical expressions that governs the entire well-to-seismic tie workflow are presented below;

$$AI = \rho v \qquad (3)$$

$$RC = \frac{\rho_2 v_2 - \rho_1 v_1}{\rho_2 v_2 + \rho_1 v_1} \qquad (4)$$

$$Synthetic\ Seismogram = \frac{\rho_2 v_2 - \rho_1 v_1}{\rho_2 v_2 + \rho_1 v_1} * wavelet \qquad (5)$$

Where ρ= Density, v =Velocity, AI= Acoustic impedance and RC = Reflection coefficient.

Faults were identified as discontinuities or breaks in the seismic reflections. Faults were mapped on both inline and cross-line directions. Horizons are continuous lateral reflection events that are truncated by fault lines. The horizon interpretation process was conducted along both inline and crossline direction. At the end of the horizon mapping, a seed grid is generated which serves as an input for time surface generation. Time surfaces were generated using the seed grids gotten from the horizon mapping process. The third order polynomial velocity model was generated and used to depth convert the time surfaces of the reservoirs of interest.

3.3. Variance (Edge Detection) Method

The variance attribute is edge imaging and detection techniques. It is used for imaging discontinuity related to faulting or stratigraphy in seismic data. Variance attribute is proven to help in imaging of channels, fault zones, fractures, unconformities and the major sequence boundaries (Pigott. et al, 2013). In the Petrel software, the variance attribute uses an algorithm that computes the local variance of the seismic data through a multi-trace window with user-defined size. The local variance is computed from horizontal sub-slices for each voxel. A vertical window was used for smoothing the computed variance and the observed amplitude normalized. The variance attribute measures the horizontal continuity of the amplitude that is the amplitude difference of the individual traces from their mean value within a gliding CMP window.

$$\sigma^2 = \frac{1}{n}\sum_{f_i=1}^{n}(x_i + x_m)^2 \qquad (6)$$

Where σ = standard deviation, σ^2 = variance, n = the number of observations, f_i = frequency, x_i = the variable, x_m = mean of x_i

3.4. Spectral Decomposition

Spectral decomposition is a frequency attribute. It involves separating and classifying seismic events within each trace based on their frequency content. Each 1D trace was decomposed from the time domain into its corresponding 2D representation in the time-frequency domain using algorithms. Once each trace was transformed

into the time-frequency domain, a band-pass filter was applied to view the amplitude of seismic data at different frequencies.

The short-time Fourier transform (STFT) spectrogram which is the squared modulus of the STFT and the spectral energy density is defined as (Cohen, 1989)

$$SP_s(t, f) = /\int_{-\infty}^{\infty} s(\tau)h(\tau - t)e^{-j2\pi f\tau}d\tau /^2 \qquad (7)$$

Where, $h(\tau - t)$ = the window function, $s(\tau)$ = the signal, SP_s = the short-time Fourier transform

j = the imaginary unit, τ = the time delay.

The relationships between the amplitude spectrum ($A(w)$) and the phase spectrum ($\gamma(w)$) of the estimated transformed signals are presented in equations 8 and 9

$$/A(w^T)/ = \sqrt{A_r + A_i} \qquad (8)$$

$$\gamma(w) = \mathrm{Tan}^{-1}[\frac{A_i}{A_r}] \qquad (9)$$

A_r = real part of $A(w^T)$, A_i = imaginary part of $A(w^T)$, w = frequency, T = transform of the signal, $A(w^T)$ = amplitude of transformed trace at frequency w.

4.0. Results and Discussion

4.1. Production Data

The Production and Reservoir Pressure Reports are presented in Figures 2 and 3. Production decline of 1192.21bbl/day resulted from pressure decline of 95.50bar/year or 0.062psi/year.

4.2. Normalized Root Mean Square (NRMS) Repeatability (RRR) and 4D Response

The NRMS of 0.38 has been achieved, in this study, implying very good repeatability when considering the quality of data and acquisition difference. The seismic time-lapse difference between the base and monitor surveys was successfully extracted. The fact of the difference from the monitor implies the existence of production induced effect and acquisition, environmental and processing noises, hence the 4D or time-lapse response signal.

4.3. Reservoir Identification, Correlation and Well-to-Seismic Ties

The results for lithology and reservoir identification are presented in Figure 4. A total of nine sand bodies (A, B, C, D, E, F, G, H and I) were identified and correlated across all seven wells in the field. Two reservoir sands were selected for the purpose of this study (Reservoirs A and I). The resistivity logs which reveals the presence of hydrocarbons were used to identify the hydrocarbon bearing sands. On Figure 4, the sands are coloured yellow while shales are grey in colour. The results for well-to-seismic tie conducted on Fuba field using density log, sonic log and checkshot of Well-1 is presented in Figure 5. A statistical wavelet (ISIS time) was used to give a near perfect match between the seismic and synthetic seismogram.

Mediterranean Journal of Basic and Applied Sciences (MJBAS)
Volume 7, Issue 2, Pages 103-115, April-June 2023

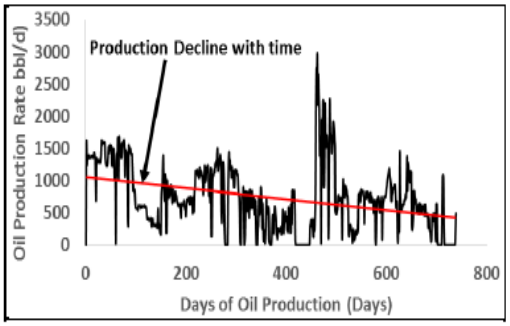

Figure 2. Reservoir Production Rate Versus Days of Oil Production

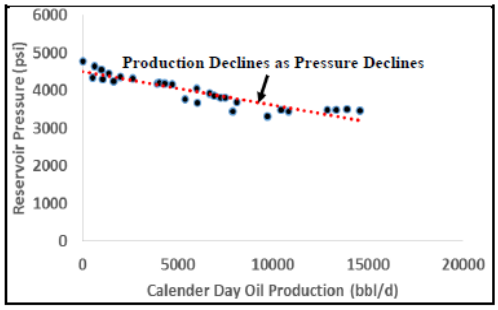

Figure 3. Effect of Reservoir Pressure Decline on Production

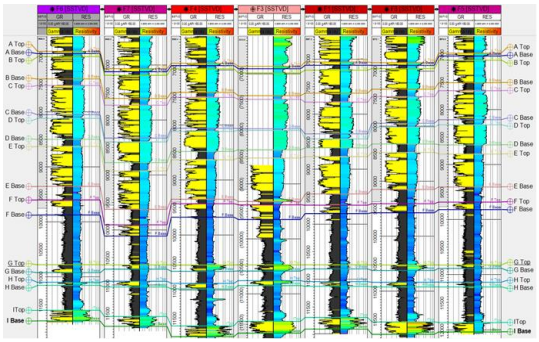

Figure 4. Well section showing reservoir identified and correlated across Fuba Field

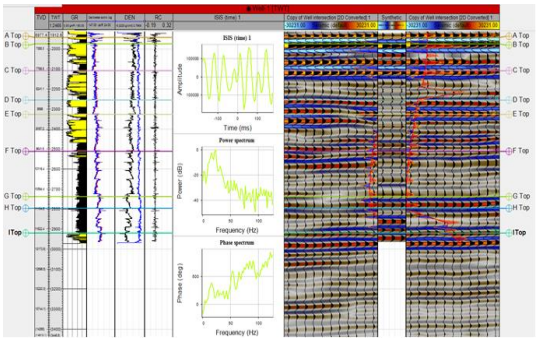

Figure 5. Synthetic seismogram generation and well-to-seismic tie conducted for Fuba Field using Well-1 Checkshot

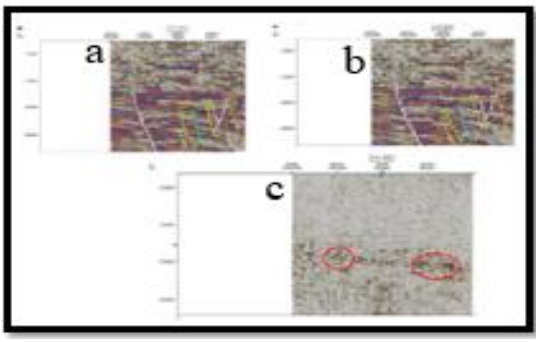

Figure 6. Base, Monitor and Difference Seismic Section for Inline 8590 Interpreted

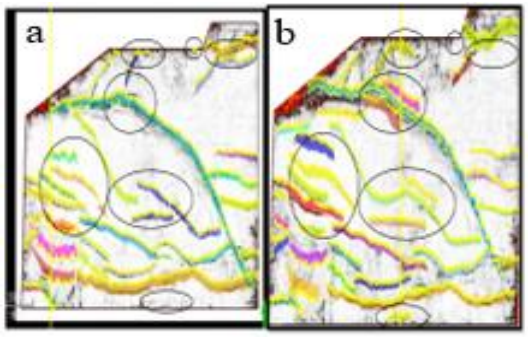

Figure 7. 4D Effect (Diffference) Betweeen Base and Monitor Interpreted Faults Displayed on the Variance Time Slice

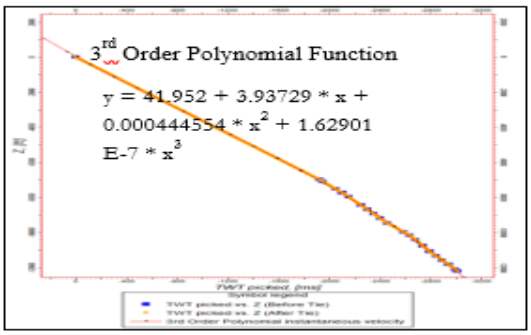

Figure 8. Third Order Polynomial Velocity model for Converting Reservoir Surfaces from Time to Depth

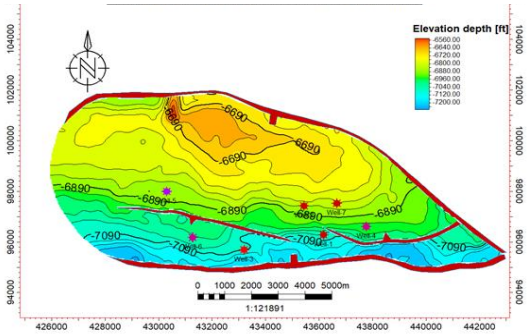

Figure 9. Reservoir Surface for Depth Surface Utilized A

Mediterranean Journal of Basic and Applied Sciences (MJBAS)
Volume 7, Issue 2, Pages 103-115, April-June 2023

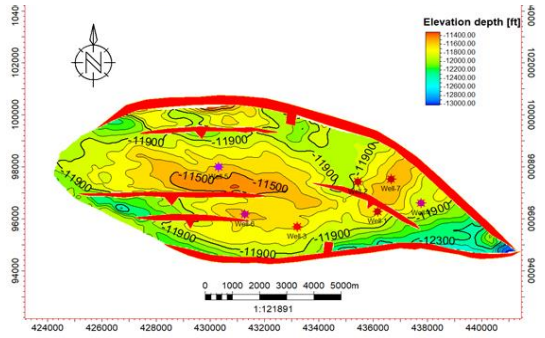

Figure 10. Reservoir Surface for Depth Surface I

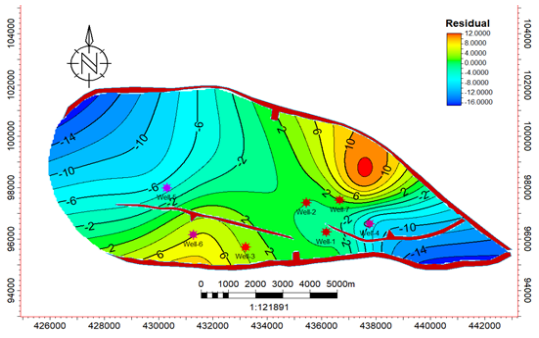

Figure 11. Depth Residual Maps Generated from Surfaces Converted Using the 3rd Order Polynomial Velocity Function for Reservoir A

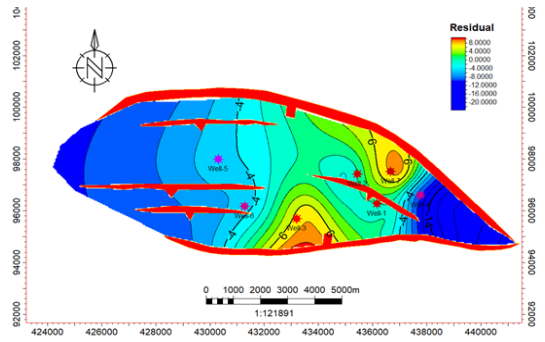

Figure 12. Depth Residual Maps Generated from Surfaces Converted Using the 3rd Order Polynomial Velocity Function for Reservoir I

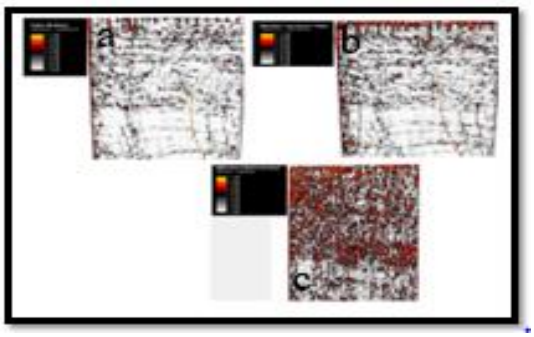

Figure 13. Variance Edge Inline 8515 for Base, Monitor and Difference Volume

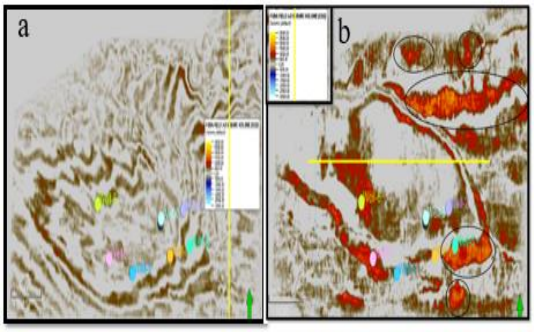

Figure 14. The General Spectral Decomposition Volume at Frequency of 12-35Hz (a) Base, (b) Monitor

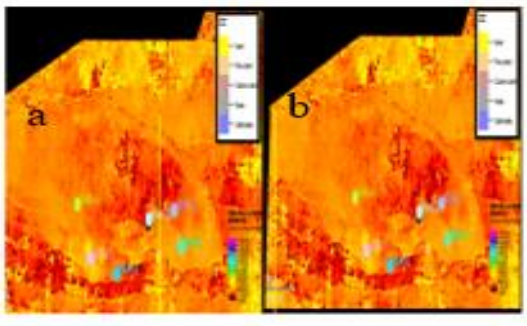

Figure 15. Spectral Decomposition at Dominant Frequency of 25Hz Volume (a) Base, (b) Monitor

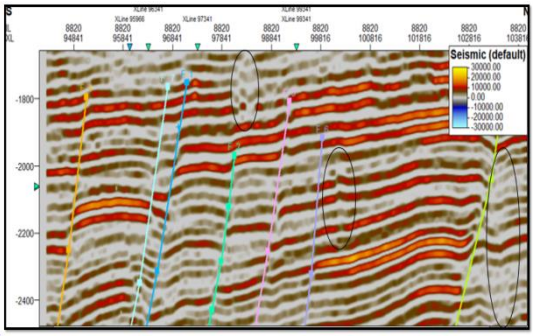

Figure 16. The General Spectral Decomposition at Frequency of 12-35Hz for Base Inline 8820

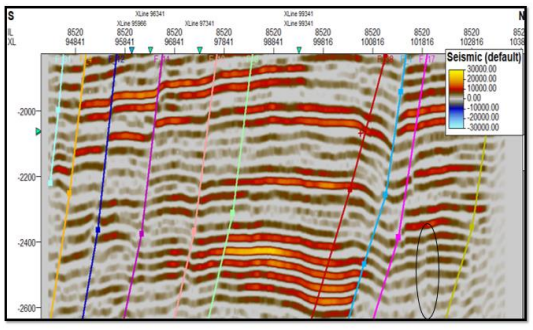

Figure 17. The General Spectral Decomposition at Frequency of 12-35Hz for Monitor Inline 8820

Mediterranean Journal of Basic and Applied Sciences (MJBAS)
Volume 7, Issue 2, Pages 103-115, April-June 2023

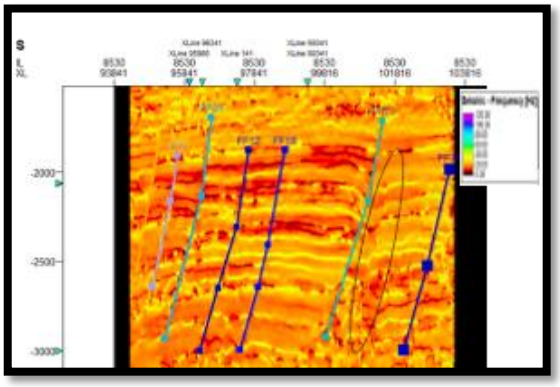

Figure 18. Spectral Decomposition at Dominant Frequency of 25Hz for Base Inline 8820

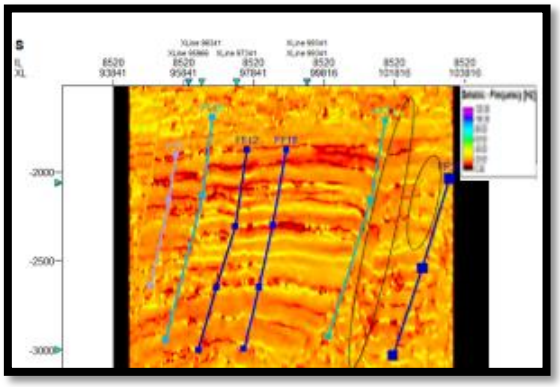

Figure 19. Spectral Decomposition at Dominant Frequency of 25Hz for Monitor Inline 8820

4.4. Fault and Horizon Interpretation

The results for the interpreted faults in Fuba field are presented in Figure 6 shows both synthetic and antithetic faults interpreted along seismic inlines. Faults are more visible along the inline direction because this direction reveals the true dip position of geologic structures. The variance time slice was used to validate the interpreted faults as shown in figure 7. The areas in black circles indicate the 4D response. All interpreted faults are normal synthetic and antithetic faults. A total of thirty-six faults were interpreted across the entire base seismic data while forty faults were interpreted across the entire monitor seismic data. Of the interpreted faults, only F1 (synthetic fault) and F16 (antithetic fault) faults are regional, running from the top to bottom across the field. Hence, these faults play significant roles in trap formation at the upper, middle and lower sections of the field. The results for the interpreted seismic horizons (Horizons A and I) are also presented in Figure 6. On these horizons, the fault polygons were generated and eliminated. The horizons were used as inputs for the generation of reservoir time surfaces.

4.5. Depth Surfaces

The result of depth conversion residual analysis is presented in Table 1. The depth residual is the difference between the depth values of the well top from each well and the depth value from the depth converted reservoir surfaces. The depth residual analysis revealed that surfaces converted using the linear velocity function had the largest residuals ranging from -31.60 to +61.67 and from -50.58 to +40.84ft in reservoir A and reservoir I respectively. This is closely followed by the residual values obtained with the 2nd order polynomial function. The third order polynomial function shows the least residuals, ranging from -6.69 to +6.61 ft in reservoir A, and -9.48 to +8.42ft respectively. The negative depth residual indicates that the depth conversion process displaces the reservoir to a greater depth than where it occurs in the subsurface, while a positive depth residual signifies that the depth converted result has placed the reservoir at a shallower depth (Ogbamikhumi and Aderibigbe, 2019). The resultant depth residual values generated using the various velocity models (linear, 2nd and 3rd order polynomials) were compared in order to select the most suitable velocity model for depth conversion of the reservoir surfaces. Figure 8 shows the 3rd order polynomial velocity model which was selected and used as most suitable velocity model for converting A and I reservoirs from time to depth because it has the least residuals. The depth converted

reservoir A and I surfaces are presented in Figures 9 and 10 for the third order polynomial velocity function. The depth structure maps reveal that the reservoirs are anticlinal and fault supported. Reservoir A is found at a shallower depth from 6500 to 7500 ft while reservoir I is found at a deeper depth ranging from 11500 to 13000ft respectively. The depth residuals recorded from the various well locations were used to generate depth residual maps which are presented in Figures 11 and 12 respectively. The depth residual maps revealed that higher residuals on reservoir A and I surfaces are associated with the eastern and western regions which are areas not penetrated by any well.

4.6. Variance Attribute

Figure 13 shows the computed variance attributes of the seismic section. The variance values range from 0.0 to 1.0. Values of variance equal to 1 represent discontinuities while a continuous seismic event is represented by the value of 0. The high values are denoted with red to yellow colorations. There are more discontinuities in figure 13c which implies that there are more cracks in the field of study due to production.

Concerning the variance map, the areas dotted with blue, green, orange and pink colored lines signify values that correspond to the location of the discontinuity. The discontinuities may be interpreted as faults and boundaries as shown by the lines drawn on the variance attribute map. The variance edge enhanced the faults or sedimentological bodies within the seismic data volume. Furthermore, several bright spots are also delineated (in black circles and black ovals) which indicate high reflectivity sediments compared to their surroundings. These bright spots are an indication that a potential hydrocarbon trap might exist in the area. The variance attribute is edge imaging and detection techniques. It is used for imaging discontinuity related to faulting or stratigraphy in seismic data. Variance attribute is proven to help in imaging of channels, fault zones, fractures, unconformities and the major sequence boundaries. The darkest regions in the seismic section, which make vertical strips, may be interpreted as faults or fractures. The zones with low variance values are due to similar seismic traces. Areas with red patches represent lineaments/discontinuities while grey areas represent the structural framework of the field.

4.7. Spectral Decomposition

The general spectral decomposition was done at a frequency of 12-35Hz for the base and the monitor seismic. Figure 14 is the seismic volume obtained for the general spectral decomposition. Figure 14 illustrates Red-Green-Blue blend of the higher resolution of the frequency of 12-35Hz. The RGB colour blend effect gives a better understanding of the geology reservoirs. The colour blend is spectral balancing which recompense for wavelet and energy loss. The figure showed a complex meandering system and other less winding channels which are discontinuous and difficult to resolve on the seismic. The RGB colour blending slices revealed more hidden structures compared with what is observed in the time structural map. In these figures, the areas in red color indicate areas of low frequency and high amplitude associated with known hydrocarbon zones and when one colour is dominating, it showed that the frequency is dominating at that point. There are more areas in red color in the monitor stack which indicates that there are more areas of low frequency and high amplitude associated with known hydrocarbon zones. It revealed the geometry of the channels and other fewer sinusoidal channels. The channels are displayed with bright colouration which contains multiple frequencies as observed within the low

frequency and indicated in black circles in Figure 14b. The meandering channels run across from the north-eastern to the south-eastern part. These are likely traps for hydrocarbon accumulation (Neuendorf, et al, 2005). The amplitude response which is dominated by blue colour is high frequency. At the central part, there is high amplitude, an indication of hydrocarbon/gas effect. The acoustic impedance within the gas-bearing sand is lower compared to the surrounding shale (Naseer, and Asim, 2017). At parts where there's a change in colour to brownish, it showed thickening up of the reflectors and greater contribution from the lower frequencies. There are colour changes in the channel system which could be indicative of changes in lithology.

The dominant frequency spectral decomposition was done at of 25Hz for the base and the monitor seismic. Figure 15 is the seismic volume obtained for the dominant frequency spectral decomposition. The yellow colored areas observed in Figure 15 indicate the presence of sand while the blue patches regions indicate the presence of shale. This suggests that the seismic volume has more sand contents.

4.8. Stratigraphic Contact

A major geologic feature was observed on the time-slice from the divergent pattern on the seismic section as we penetrate deeper, which is an unconformity (Figures 16 and 17). This represents a significant break in vertical velocity or breaks in deposition time or record on horizon (Neuendorf, et al, 2005). This type of unconformity is called angular unconformity. Angular unconformity is an unconformity between two groups of rocks whose bedding planes are not parallel or in which the older underlying rock dips at a different angle (usually steeper) than the younger, overlying strata. Its interpretation depends on the recognition of characteristic reflection geometries rather than on amplitude information. It shows that deposition of the sediments took place at different times. Some of the lobes are indicated in Figures 16 and 17 (individual lobes I, J, K and L).

As can be seen in the areas in black ovals in the Figures 16, 17, 18 and 19, the results of spectral decomposition at the different frequencies indicates the following: (a) There are more faults within the field than previously interpreted resulting in a more complex structure; (b) There is more continuity of fault than previously interpreted; (c) The presence of small scale faults and lobes in the field.

Table 1. Depth Residual between Well Tops and Resultant Depth Surfaces

Reservoir/ Well	**Well Top (ft)**	**Depth Surface (ft)**	**Difference (ft)**	**Depth Surface (ft)**	**Difference (ft)**	**Depth Surface (ft)**	**Difference (ft)**
		Linear Velocity Function		***2nd Order Polynomial***		***3rd Order Polynomial***	
Reservoir A Well-1	-7054.07	-7079.08	25.01	-7032.58	-21.49	-7053.13	-0.95
Well-2	Missing	Missing	Missing	Missing	Missing	Missing	Missing
Well-3	-6877.06	-6849.08	-27.98	-6886.40	9.34	-6880.86	3.80
Well-4	-6977.93	-7039.60	61.67	-7004.73	26.80	-6971.24	-6.69
Well-5	-6905.39	-6873.79	-31.60	-6859.58	-45.81	-6900.65	-4.74

Well-6	-7065.18	-7105.10	39.92	-7028.91	-36.27	-7070.87	5.69
Well-7	-6846.24	-6877.44	31.20	-6854.65	8.41	-6852.85	6.61
Reservoir I Well-1	-11690.91	-11720.12	29.21	-11674.22	-16.69	-11690.91	0.00
Well-2	-11823.41	-11780.54	-42.87	-11807.54	-15.87	-11823.41	0.00
Well-3	-11650.06	-11684.44	34.38	-11666.36	16.30	-11656.67	6.61
Well-4	-11887.08	-11845.26	-41.82	-11912.42	25.34	-11877.60	-9.48
Well-5	-11599.86	-11549.01	-50.85	-11581.29	-18.57	-11595.11	-4.75
Well-6	-11569.00	-11534.94	-34.06	-11586.60	17.60	-11564.27	-4.73
Well-7	-11551.91	-11592.75	40.84	-11534.64	-17.27	-11560.33	8.42

5.0. Conclusion

Production decline of 1192.21bbl/day resulted from pressure decline of 95.50bar/year or 0.062psi/year. Most of the data points were not repeatable as evidenced in the computed Normalized root mean square (NRMS) of 0.38 meaning that on 62.0% of Base and Monitor data points were coincident. A total of nine sand bodies (A, B, C, D, E, F, G, H and I) were identified and correlated across all seven wells in the field. Two horizons (A and I) were selected for the study. Structural interpretation of seismic data revealed that the field is highly faulted with synthetic and antithetic faults which are in line with faults trends identified in the Niger Delta. Fault and horizon interpretation revealed that closures found are collapsed crestal structures bounded by two major faults. The depth structure maps reveal anticlinal faults. Reservoirs are found at a shallower depth from 6500 to 7500 ft and at a deeper depth ranging from 11500 to 13000ft. The synthetic and antithetic faults act as good traps for the hydrocarbon accumulation in the study area. The variance values range from 0.0 to 1.0 The Variance edge analysis was used to delineate the prominent and subtle faults in the area. There are more discontinuities in the difference volume variance edge which implies that there are more cracks in the field of study due to production. The results of spectral decomposition at the different frequencies indicates the following: (a) areas of low frequency and high amplitude associated with known hydrocarbon zones; (b) There are more faults within the field than previously interpreted resulting in a more complex structure; (c) There is more continuity of faults than previously interpreted; (d) The presence of small scale faults and lobes in the field; (e) The presence of channels in the field. The result showed the validity of the technique and can also be used to propose a new drilling site. Modern exploration technology with enhanced oil recovery techniques can be successfully adopted to harness the hydrocarbon in these by-passed zones where drilling was once uneconomic. This will further lead to an increase in the productivity within the field. Finally, it is recommended that further studies should be done on the application of time-frequency decomposition for stratigraphic interpretation of thin sandstone reservoirs in the study area.

Declarations

Source of Funding

This study did not receive any grant from funding agencies in the public or not-for-profit sectors.

Competing Interests Statement

The author has declared no competing interests.

Consent for Publication

The author declares that she consented to the publication of this study.

Acknowledgements

The author is grateful to Shell Petroleum Development Company of Nigeria (SPDC), Port Harcourt Nigeria for the release of the academic data for the purpose of this study.

References

[1] Sheriff, R.E. (2002). Encyclopaedic Dictionary of Applied Geophysics, Fourth Edition, Society of Exploration Geophysicists.

[2] Bayowa, G.O., Adagunodo A.T., Oshonaiye O.A. & Boluwade, S.B. (2021). Mapping of Thin Sandstone Reservoirs in Bisol Field, Niger Delta, Nigeria Using Spectral Decomposition Technique. Geodesy and Geodynamics, 12: 54–64.

[3] Naseer, M.T. & Asim S. (2018). Characterization of Shallow –marine Reservoirs of Lower Eocene Carbonates, Pakistan: Continuous Wavelet Transforms-based Spectral Decomposition. Journal of Natural Gas, Science and Engineering, 56: 629–649.

[4] Tayyab M.N., Asim, S.Siddiqui M.M., Naeem, M., Solange, S.H. & Babar F.K. (2017). Seismic Attributes Application to Evaluate the GoruClastics of Indus Basin, Pakistan. Arab Journal of Geoscience, 10(7): 158.

[5] Cohen, L. (1995). Time Frequency Analysis, Prentice Hall, New Jersey.

[6] Castagna, J.P. & Sun, S. (2006). Comparison of Spectral Decomposition Methods. First Break, 24: 3–24.

[7] Taner, M.T., Koehler, F. & Sheriff, R.E. (1979). Complex Seismic Trace Analysis. Geophysics, 44: 1041–1063.

[8] Marfurt, K.J. & Kirlin R.L. (2001). Narrow-band Spectral Analysis and Thin-Bed Tuning. Geophysics, 66: 1274–1283.

[9] Castagna, J.P., Sun, S. & Siegfried, R.W. (2003). Instantaneous Spectral Analysis; Detection of Low-frequency Shadows Associated with Hydrocarbons. Leading Edge, 22: 120–127.

[10] Sinha, S., Routh, P.S. & Anno, P.D. (2005). Spectral Decomposition of Seismic Data with Continuous Wavelet Transform. Geophysics, 70: 19–25.

[11] Tomasso, M., Bouroullec, R. & Pyles D.R. (2010). The Use of Spectral Recomposition in Tailored Forward Seismic Modelling of Outcrop Analogs. AAPG Bulletin, 94: 457–474.

[12] Whiteman, A. (1982). Nigeria: Its Petroleum Ecology Resources and Potential. London, Graham and Trotman.

[13] Adegoke, O.S., Oyebamiji, A.S., Edet, J.J, Osterloff, P.L. & Ulu, O.K (2017). Cenozoic Foraminifera and Calcareous Nannofossil Biostratigraphy of the Niger Delta. Elsevier, Cathleen Sether, United States.

[14] Short, K.C. & Stable A.J. (1967). Outline of Geology of Niger Delta. Bulletin of America Association of Petroleum Geologists, 51(5): 761–779.

[15] Horsfall, O.I., Uko, E.D., Tamunoberetonari I. & Omubo-Pepple, V.B. (2017). Rock-Physics and Seismic-Inversion Based Reservoir Characterization of AKOS FIELD, Coastal Swamp Depobelt, Niger Delta, Nigeria. IOSR Journal of Applied Geology and Geophysics, 5(4): 59–67.

[16] Ochoma, U., Uko E.D. & Horsfall, O.I. (2020). Deterministic Hydrocarbon Volume Estimation of the Onshore Fuba Field, Niger Delta, Nigeria. IOSR Journal of Applied Geology and Geophysics, 8(1): 34–40.

[17] Vedanti, N., Pathak, A., Srivastava, R.P. and Dimri, V.P. (2009). Time Lapse (4D) Seismic: Some Case Studies. e-Journal Earth Science India, 2(4): 230–248.

[18] Varela, O.J., Torres-verdin, C., Sen, M.K. and Roy, I.G. (2006). Using Time-lapse Seismic Amplitude Data to Detect Variations of Pore Pressure and Fluid Saturation Due to Oil Displacement by Water: A Numerical Study Based on One-Dimensional Prestack Inversion. Journal of Geophysics and Engineering, 3: 177–193.

[19] Kragh, E. & Christie, P. (2002). Seismic Repeatability, Normalized Rms, and Predictability. The Leading Edge, 21(7): 640–647.

[20] Johnston, D.H. (2013). Practical Applications of Time-lapse Seismic Data. SEG Distinguished Instructor Series No.16, SEG.

[21] Pigott. J.D., Kang, M.I.H. & Han, H.C. (2013). First Order Seismic Attributes for Clastic Seismic Facies Interpretation: Examples from the East China Sea. Journal of Asian Earth Science, 66: 34–54.

[22] Cohen L. (1989). Time-frequency Distributions-a Review. Proc. IEEE, Pages 941-981.

[23] Ogbamikhumi, A. & Aderibigbe, T.O. (2019). Velocity Modelling and Depth Conversion Uncertainty Analysis of Onshore Reservoirs in the Niger Delta Basin. Journal of the Cameroon Academy of Sciences, 14(3): 239–247.

[24] Neuendorf, K.K.E., Mehl, J.P. & Jackson, J.A. (2005). Glossary of Geology, Fifth Edition. American Geological Institute, Alexandria, Virginia, Page 779.

[25] Naseer, M.T., Asim, S. (2017). Detection of Cretaceous Incised Valley Shale for Resource play, Miano gas field, SW Pakistan: Spectral Decomposition Using Continuous Wavelet Transform. Journal of Asian Earth Science, 147: 358–377.